Fixing the Energy Scale in Scanning Tunneling Microscopy on Semiconductor Surfaces

Gerhard Münnich,[1] Andrea Donarini,[2] Martin Wenderoth,[3] and Jascha Repp[1]

[1]*Institute of Experimental and Applied Physics, University of Regensburg, 93053 Regensburg, Germany*
[2]*Institute of Theoretical Physics, University of Regensburg, 93053 Regensburg, Germany*
[3]*IV. Physikalisches Institut der Georg-August-Universität Göttingen, Friedrich-Hund-Platz 1, 37077 Göttingen, Germany*

(Received 17 May 2013; published 19 November 2013)

In scanning tunneling experiments on semiconductor surfaces, the energy scale within the tunneling junction is usually unknown due to tip-induced band bending. Here, we experimentally recover the zero point of the energy scale by combining scanning tunneling microscopy with Kelvin probe force spectroscopy. With this technique, we revisit shallow acceptors buried in GaAs. Enhanced acceptor-related conductance is observed in negative, zero, and positive band-bending regimes. An Anderson-Hubbard model is used to rationalize our findings, capturing the crossover between the acceptor state being part of an impurity band for zero band bending and the acceptor state being split off and localized for strong negative or positive band bending, respectively.

DOI: 10.1103/PhysRevLett.111.216802 PACS numbers: 73.40.Gk, 71.55.Eq, 73.20.−r, 73.40.Qv

Since its invention, the scanning tunneling microscope (STM) has been widely used to study semiconductor surfaces. The qualitative interpretation of such studies can be obscured by the presence of tip-induced band bending TIBB(V), i.e., by the bias-dependent shift of all electronic states beneath the microscope's tip [1–3]. If shifted across the Fermi level, TIBB(V) changes the average occupation of an electronic state, which, in turn, determines if this state contributes to the electronic transport within the junction [4–8]. However, since the contact potential difference (CPD) between tip and sample is, with few exceptions [9,10], unknown in STM, within the relevant bias range, not even the sign of TIBB(V) is known. In this context, the conductance spectra of shallow acceptors buried in III–V semiconductor hosts remained a puzzle unsolved for almost two decades: depending on the sign of the band bending assumed or inferred from scanning tunneling spectroscopy (STS), conductance is explained either due to tunneling of electrons into empty acceptor states (positive TIBB) [11], or due to a modification of the tunneling barrier by the occupied acceptor (negative TIBB) [12], or by the empty acceptor state being in resonance with an impurity band (zero TIBB) [13]. Although the need for an exact value of the CPD has clearly been recognized [12,13], bare STM-based methods used so far seem not to be sufficient to resolve this puzzle.

To this end, we combine STM on a semiconducting surface with Kelvin probe force spectroscopy (KPFS) [14], which allows an independent and direct measurement of the CPD, which fixes the polarity of TIBB(V) for all voltages. With this combination, we revisit the shallow acceptor Zn buried in GaAs [11–13,15,16]. Our method reveals that the enhanced conductance induced by shallow acceptors is not only present in one single band-bending regime, as argued in previous publications [11–13], but *similarly* in the regimes of negative, zero, and positive TIBB(V).

The spatially localized band bending in an STM setup will split off the foremost acceptor state from an impurity band. In the most simple picture [11–13], this state was treated as being isolated. However, for small TIBB(V), this state is still part of the delocalized impurity band, and only with increasing TIBB(V) is it gradually becoming split off and isolated. The increasing localization of the state will affect its charging energy, which may become relevant when considering charge transport. Hence, not only TIBB(V) itself but also the *effective* electronic coupling and the charging energy of the acceptor state change with increasing bias voltage during spectra acquisition. Additionally, the band bending will affect more than just a single acceptor. Accordingly, we treat the electronic transport within the junction using an Anderson-Hubbard model for the foremost acceptor states which are affected by TIBB(V).

Experiments were performed by means of a combined STM and atomic force microscope, which was operated in ultrahigh vacuum at a temperature of $\sim$5 K, using a qPlus force sensor equipped with a Pt/Ir tip [17]. As samples, we use commercially available GaAs wafers, which are cleaved *in situ* to expose the (110) surface. The samples are p type doped with Zn, at an average dopant concentration of 1×10^{19} cm^{-3}, which establishes an impurity band of 24 meV width, centered around 31 meV above the valence-band edge [18]. This concentration corresponds to an average nearest-neighbor acceptor distance of ≈ 45 Å and a penetration depth of the field of roughly twice this length [19]. Assuming a tip radius of $\gtrsim 150$ Å, we expect about ten acceptors to be located within the TIBB-induced space-charge region [20].

Figure 1 shows STM and KPFS measurements performed with three different tip apices. These have been changed by controlled indentation into a clean Cu(111) surface. In the following, we will discuss data acquired

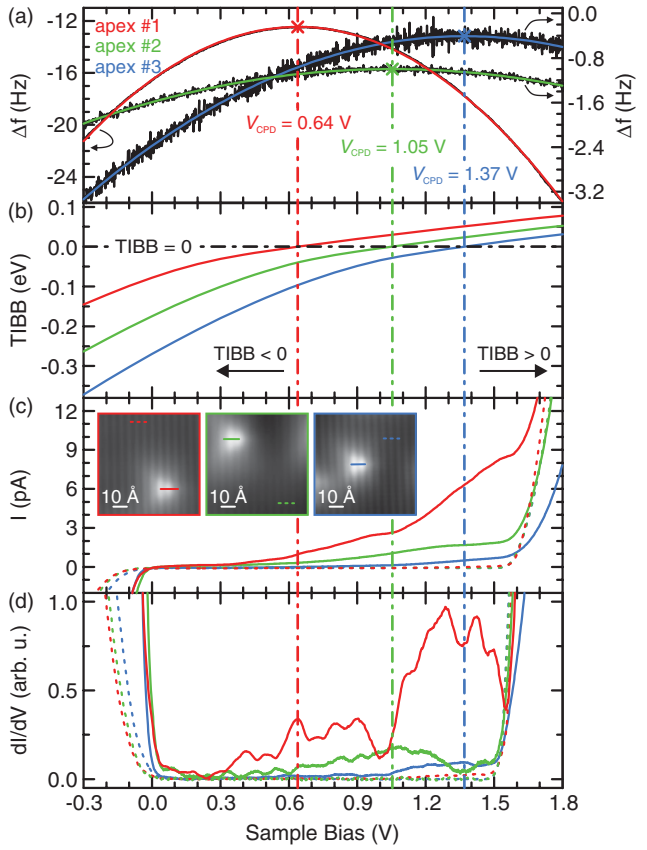

FIG. 1 (color). Contact potential difference and acceptor-induced conductance for different tip apices. (a) Frequency shifts measured as a function of sample bias $\Delta f(V)$ (black lines), parabolic fits, and the corresponding flat-band voltages V_{CPD} are indicated (colored lines). (b) Calculated tip-induced band bending. For any sample bias below (above) V_{CPD}, the band bending is negative (positive). (c),(d) $I(V)$ and $dI/dV(V)$ spectra away from (dashed lines) and atop (solid lines) subsurface acceptors; positions are indicated in the constant-current STM images (inset: $V = 1.5$ V, $I = 20$ pA). For all tip apices, acceptor-induced enhanced current and conductance are observed in negative, zero, and positive band-bending regimes.

with tip apex #1 (red lines in Fig. 1) while showing the results for three different tip apices to underscore the general validity of our findings. Figure 1(a) shows KPFS data. In KPFS, the frequency shift $\Delta f(V)$ of the force sensor is recorded as a function of the dc sample bias V at a fixed tip position. The electrostatic contribution to the force between tip and sample gives rise to a parabolic dependence of $\Delta f(V)$ with V as $\Delta f(V) \propto -(V - V_{\mathrm{CPD}})^2$ [21]. For compensated CPD, that is, for $V = V_{\mathrm{CPD}}$, the electrostatic field in the tip-sample junction will be zero and $\Delta f(V)$ will be maximal, respectively. In this situation, there is no electric field to penetrate the semiconductor and hence V_{CPD} is the flat-band voltage [22]. From the parabolic fit to $\Delta f(V)$ [cf. Fig. 1(a)], we extract a flat-band voltage of $+0.64$ V for tip apex #1 [23]. The assignment of V_{CPD} to the flat-band condition relies on the GaAs(110) surface not being subject to Fermi-level pinning, our cleaved surface being atomically flat, and our sample being homogeneous and well conducting at 5 K. As this assignment is the key to our experiments, its uncertainty was quantified as follows. (i) Performing KPFS on GaAs at a set of different tip-sample distances showed that local variations of the work function [24] of the tip apices used contribute to this uncertainty only by about ± 30 meV, and (ii) we measured V_{CPD} values on GaAs(110) and on clean Cu(111) with the same tip apices and compared the differences to the values expected from literature [20]. This provides a generous upper bound for the uncertainty of the absolute value of V_{CPD} of 0.12 eV [25,26], which is still small compared to the voltage scales considered here. Finally, we note that tunneling current vs tip-sample distance $[I(z)]$ spectra acquired additionally do not result in correct or self-consistent CPD values [20,27].

As TIBB(V) is a monotonic function of the applied sample bias, shifted with respect to zero bias by the CPD, we can attribute a negative (positive) TIBB(V) to any sample bias below (above) $+0.64$ V, and TIBB$(0.64\ \mathrm{V}) = 0$ for tip apex #1. The voltage dependence of TIBB(V) is shown in Fig. 1(b), where we used V_{CPD} as an input parameter to a one-dimensional Poisson-equation solver developed by Feenstra [28]. The flat-band voltage [and the corresponding zero crossing of TIBB(V)] is indicated by a vertical (horizontal) dash-dotted line. We point out that the magnitude of TIBB(V) is still uncertain, as it depends on the geometry of the tip, which cannot be easily extracted from KPFS.

Now, we investigate the electronic transport through Zn acceptors buried below the GaAs(110) surface by means of STS in view of the experimentally determined CPD for tip apex #1. Figures 1(c) and 1(d) show (spatially averaged) $I(V)$ and differential conductance $[dI/dV(V)]$ spectra, recorded away from and atop a subsurface acceptor, as is indicated by the colored lines in the constant-current topography shown in the inset. Both spectra show p-type semiconducting characteristics, with a valence-band-related current onset below 0 V and a conduction-band-related current onset above 1.5 V. In contrast to the spectra as acquired away from the acceptor, the spectra acquired atop the Zn acceptor also show nonzero current and conductance within a large bias interval located within the semiconducting band gap. Whereas this has been reported before [11–13], the nonzero conductance has so far never been related to quantitative contact potential difference measurements. For this particular tip apex, the flat-band condition has been unambiguously determined to be $+0.64$ V; therefore we immediately see that acceptor-related conductance is present for negative, zero, and positive TIBB(V). The same holds true for data acquired with tip apices #2 and #3 which show distinctly different values of the CPD (1.05 and 1.37 eV, respectively); see Fig. 1.

To map out the spatial dependence of the acceptor-related enhanced conductance, we have recorded differential

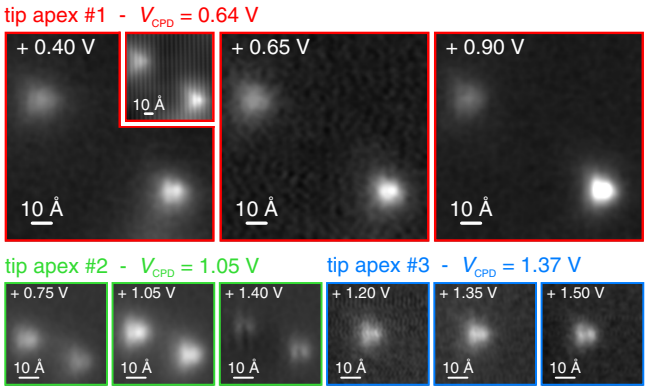

FIG. 2 (color online). dI/dV maps of subsurface acceptors acquired with tip apices #1 (inset: constant-current topography, $V = 1.5$ V, $I = 20$ pA) to #3. For each apex, maps are acquired at voltages below, at, and above the corresponding flat-band voltage (sample biases as indicated; the gray scale is identical for each apex). For all apices, within all band-bending regimes, a similar triangular feature of enhanced conductance is observed.

conductance maps. In Fig. 2, we show dI/dV maps acquired with tip apices #1 to #3, recorded at bias voltages well below, right at, and well above the corresponding flat-band voltage. In accordance with previous experiments, we observe a triangular feature of enhanced conductance at the position of the dopant atom [11]. Most notably, for all apices, a similar pattern of enhanced conductance is observed for negative, zero, and positive band bending. The similarity present in different band-bending regimes suggests that *one* conduction mechanism is responsible for all of them. Most importantly, the polarity of the sample bias of the differential conductance maps for all three band-bending regimes remains the same, such that the occurrence of the same conduction mechanism is not related to bipolar tunneling [10,11,29]. The basis of most pictures used so far in this context is a single *isolated* acceptor level being shifted by TIBB(V) against the Fermi level. In this picture, the occupation of the level has to change when shifted across the Fermi level, which determines whether or not a particular channel can contribute to transport, independent of the further details of the model [12,13]. Hence, in these pictures, no transport mechanisms can be active in *all* three regimes for one particular sample bias polarity. However, our conductance spectra, related to the flat-band voltage, in combination with the dI/dV maps, indeed suggest that one conduction mechanism is active in all three regimes.

To resolve this controversy, we treat the system as a linear chain of N equidistant acceptor states between the microscope's tip and the bulk of the sample; see the inset of Fig. 3(a). In this picture, three energies are important for the description. (i) The band bending shifts the on-site energy ϵ_i of each acceptor state, depending on its position below the surface. This shift is zero deep inside the bulk and is assumed to increase quadratically towards the surface, where it reaches TIBB(V) as plotted in Fig. 1(b). (ii) Adjacent acceptor states are coupled via a hopping parameter t, which we have taken, in accordance with the impurity-band width of about 20 meV, to be $t = 5$ meV. (iii) In our system, the on-site Coulomb energy U of an isolated acceptor is estimated to be on the order of 10 meV, given a size of the acceptor state of about 20 Å and a dielectric constant of GaAs of about 13 [30–32]. The Hamiltonian in the Anderson-Hubbard model reads [33–35]

$$H = \sum_{i=1}^{N}\sum_{\sigma}\epsilon_i c_{i\sigma}^{\dagger}c_{i\sigma} - t\sum_{i=1}^{N-1}\sum_{\sigma}(c_{i\sigma}^{\dagger}c_{i+1\sigma} + c_{i+1\sigma}^{\dagger}c_{i\sigma}) + U\sum_{i=1}^{N}\left(c_{i\uparrow}^{\dagger}c_{i\uparrow} - \frac{1}{2}\right)\left(c_{i\downarrow}^{\dagger}c_{i\downarrow} - \frac{1}{2}\right), \quad (1)$$

where $c_{i\sigma}^{\dagger}$ creates and $c_{i\sigma}$ annihilates an electron of spin σ on the ith acceptor. Here, we choose $N = 5$ [20]. The rest of the acceptor states and the valence and the conduction bands have been modeled as an electron bath with the respective densities of states. The metallic tip has been treated analogously, having a constant density of states. Further, we assume that the tunneling between tip and acceptors is restricted to the most superficial acceptor [cf. the inset of Fig. 3(a)]. All foremost acceptors are coupled to the bulk of the sample. We note that energy dissipation is expected to occur via the inelastic excitation of vibrons [36]. The dynamics of the system is understood as a sequence of tunneling events from (to) the tip or the bulk of the sample which increase (reduce) by 1 the number of electrons populating the foremost acceptors. The method of choice for the description of these sequential tunneling dynamics is thus the master equation approach [20]. In accordance with the experimental situation, the tunneling rate Γ^T to and from tip states is by far the smallest, and thus the foremost acceptors are essentially in equilibrium with

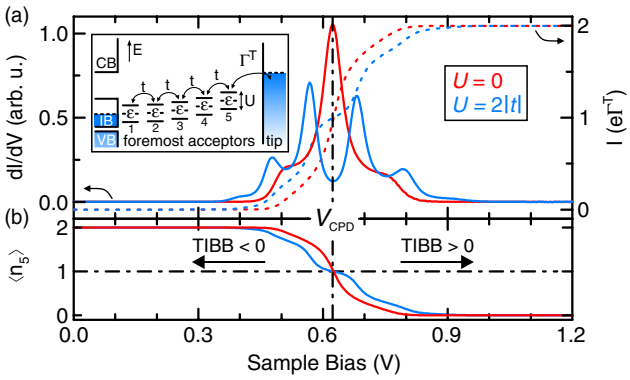

FIG. 3 (color online). Simulated electron transport within the junction. (a) Calculated $I(V)$ (dashed lines) and $dI/dV(V)$ (solid lines) spectra for vanishing ($U = 0$) and nonvanishing on-site Coulomb energy ($U = 2|t|$). The simulation yields nonzero current and conductance in a broad voltage range including negative, zero, and positive band bending. The inset sketches the relevant energies of the single-particle levels used as input for the many-body calculations. (b) Calculated average population $\langle n_5\rangle$ of the foremost acceptor.

the bulk. Moreover, for $V \approx V_{\mathrm{CPD}}$, electrons cannot tunnel from the foremost acceptors to the tip since all transport resonant levels lie far below the tip's Fermi level. Under these assumptions, the current through the system takes the form $I = e\Gamma^T(2 - \langle n_N \rangle)$, where $\langle n_N \rangle$ is the average occupation of the most superficial acceptor [see Fig. 3(b)].

This many-body approach ensures that the *gradual change* of (i) the effective electronic coupling, (ii) the localization, and (iii) the charging energy of the relevant states as a function of bias voltage is inherently captured. Figure 3(a) shows the simulated $I(V)$ and $dI/dV(V)$ spectra for different values of U. Neglecting charging energy ($U = 0$), it shows enhanced current and conductance within a large bias range in different band-bending regimes, for one sample bias polarity only, which is in accordance with our experimental findings. This phenomenon can be understood as follows. For $V \simeq V_{\mathrm{CPD}}$, $\mathrm{TIBB}(V)$ is smaller than the impurity-band width, and hence the foremost acceptor state is still part of the impurity band, even if slightly detuned from the bulk impurity states. In this voltage region, the Fermi level still remains inside this impurity band that extends to the foremost acceptor, and hence, finite conductance is observed. The size of this bias voltage range around V_{CPD} is given by the impurity-band width $4t$ divided by the lever arm $\alpha = \mathrm{TIBB}(V)/V$. For $U \neq 0$, several peaks and dips appear in the spectra as opposed to just a single broad peak that is observed for $U = 0$. Close to V_{CPD}, the single occupation of the foremost acceptor prevails until $|\mathrm{TIBB}(V)|$ overcomes $U/2$. Hence, the average population and the current develop a plateau around V_{CPD} of width U divided by α. Slight modifications in the on-site energies ϵ_i and in the tunneling coupling t_{ij} between adjacent states i and j result in variations of the relative peak heights as well as their positions with respect to V_{CPD} [20].

The simulated spectra in Fig. 3(a) are in qualitative agreement with our experimental ones [37], showing enhanced conductance in all three band-bending regimes. The experimental spectra show enhanced conductance over an even wider bias range than our theory predicts. Whereas U and α may differ from the values anticipated here, we note that electron-vibration coupling [36] could also play an important role, the incorporation of which goes beyond the scope of our model.

Finally, we note that the knowledge of the CPD in our experiments also sheds new light onto the interpretation of the observation of charge density oscillations around acceptors [16], as is discussed in the Supplemental Material [20].

In summary, the use of combined STS and KPFS allows us to unambiguously relate the conductance properties of shallow acceptors buried in GaAs to the energy scale of the system, by measuring the flat-band voltage. These measurements show that the voltage range of enhanced acceptor-induced conductance spans three different band-bending regimes, ruling out previous conceptions of electronic transport used in this context [11–13]. This experimental finding requires a theoretical description which inherently captures the crossover between the acceptor state being part of an impurity band for zero band bending and the acceptor state being split off and localized for strong negative or positive band bending, respectively. Transport calculations based on an Anderson-Hubbard model yield spectra in qualitative agreement with our experiments. We expect that this combination of Kelvin probe and scanning tunneling spectroscopy can shed new light on the energetics in cross-sectional STM experiments far beyond the specific model system studied here.

The authors thank S. Rolf-Pissarczyk, D. Gohlke, F. J. Giessibl, and M. Morgenstern for valuable discussions and M. Utz, M. Neu, and A. Pöllmann for instrumentation support. Funding from the Volkswagen Foundation (Lichtenberg Program) and the Deutsche Forschungsgemeinschaft (SFB 689, SPP 1243, and SPP 1285) is gratefully acknowledged.

[1] R. M. Feenstra and J. A. Stroscio, J. Vac. Sci. Technol. B **5**, 923 (1987).
[2] M. McEllistrem, G. Haase, D. Chen, and R. J. Hamers, Phys. Rev. Lett. **70**, 2471 (1993).
[3] J. K. Garleff, A. P. Wijnheijmer, and P. M. Koenraad, Semicond. Sci. Technol. **26**, 064001 (2011).
[4] F. Marczinowski, J. Wiebe, J.-M. Tang, M. E. Flatté, F. Meier, M. Morgenstern, and R. Wiesendanger, Phys. Rev. Lett. **99**, 157202 (2007); F. Marczinowski, J. Wiebe, F. Meier, K. Hashimoto, and R. Wiesendanger, Phys. Rev. B **77**, 115318 (2008).
[5] K. Teichmann, M. Wenderoth, S. Loth, R. G. Ulbrich, J. K. Garleff, A. P. Wijnheijmer, and P. M. Koenraad, Phys. Rev. Lett. **101**, 076103 (2008).
[6] D. H. Lee and J. A. Gupta, Science **330**, 1807 (2010).
[7] H. Zheng, J. Kröger, and R. Berndt, Phys. Rev. Lett. **108**, 076801 (2012).
[8] S. R. Schofield, P. Studer, C. F. Hirjibehedin, N. J. Curson, G. Aeppli, and D. R. Bowler, Nat. Commun. **4**, 1649 (2013).
[9] R. Dombrowski, C. Steinebach, C. Wittneven, M. Morgenstern, and R. Wiesendanger, Phys. Rev. B **59**, 8043 (1999).
[10] K. Hashimoto, C. Sohrmann, J. Wiebe, T. Inaoka, F. Meier, Y. Hirayama, R. A. Römer, R. Wiesendanger, and M. Morgenstern, Phys. Rev. Lett. **101**, 256802 (2008).
[11] G. Mahieu, B. Grandidier, D. Deresmes, J. P. Nys, D. Stiévenard, and Ph. Ebert, Phys. Rev. Lett. **94**, 026407 (2005).
[12] S. Loth, M. Wenderoth, L. Winking, R. G. Ulbrich, S. Malzer, and G. H. Döhler, Phys. Rev. Lett. **96**, 066403 (2006); S. Loth, M. Wenderoth, R. G. Ulbrich, S. Malzer, and G. H. Döhler, Phys. Rev. B **76**, 235318 (2007).
[13] A. P. Wijnheijmer, J. K. Garleff, M. A. v. d. Heijden, and P. M. Koenraad, J. Vac. Sci. Technol. B **28**, 1086 (2010).
[14] M. Nonnenmacher, M. P. O'Boyle, and H. K. Wickramasinghe, Appl. Phys. Lett. **58**, 2921 (1991).
[15] Z. F. Zheng, M. B. Salmeron, and E. R. Weber, Appl. Phys. Lett. **64**, 1836 (1994).

[16] R. de Kort, M. C. M. M. van der Wielen, A. J. A. van Roij, W. Kets, and H. van Kempen, Phys. Rev. B **63**, 125336 (2001); R. de Kort, W. Kets, and H. van Kempen, Surf. Sci. **482–485**, 495 (2001).
[17] F. J. Giessibl, Appl. Phys. Lett. **76**, 1470 (2000).
[18] E. F. Schubert, *Doping in III–V Semiconductors* (Cambridge University Press, Cambridge, England, 1993), p. 23, p. 44, and p. 186.
[19] R. M. Feenstra, J. Vac. Sci. Technol. B **21**, 2080 (2003).
[20] See Supplemental Material at http://link.aps.org/supplemental/10.1103/PhysRevLett.111.216802 for details on the experimental setup, on the determination of the uncertainty of KPFS, for a comparison of KPFS with $I(z)$ spectra, for a detailed description of the Anderson-Hubbard model, and for a discussion of charge density oscillations around acceptors.
[21] *Kelvin Probe Force Microscopy*, edited by S. Sadewasser and Th. Glatzel (Springer, Heidelberg, 2011), Vol. 48, p. 11 and p. 134.
[22] Y. Rosenwaks, R. Shikler, Th. Glatzel, and S. Sadewasser, Phys. Rev. B **70**, 085320 (2004).
[23] The standard deviations are below 7 mV.
[24] F. Krok, K. Sajewicz, J. Konior, M. Goryl, P. Piatkowski, and M. Szymonski, Phys. Rev. B **77**, 235427 (2008).
[25] Ch. Sommerhalter, Th. W. Matthes, Th. Glatzel, A. Jäger-Waldau, and M. Ch. Lux-Steiner, Appl. Phys. Lett. **75**, 286 (1999).
[26] W. Melitz, J. Shen, S. Lee, J. S. Lee, A. C. Kummel, R. Droopad, and E. T. Yu, J. Appl. Phys. **108**, 023711 (2010).
[27] T. König, G. H. Simon, H.-P. Rust, and M. Heyde, J. Phys. Chem. C **113**, 11 301 (2009).
[28] The calculation was performed using the SEMITIP software, version 6, www.andrew.cmu.edu/user/feenstra/, using an absolute tip-sample distance of 10 Å.
[29] S. W. Wu, G. V. Nazin, X. Chen, X. H. Qiu, and W. Ho, Phys. Rev. Lett. **93**, 236802 (2004).
[30] S. Adachi, *GaAs and Related Materials* (World Scientific, Singapore, 1999), p. 115.
[31] H. Kamimura and H. Aoki, *The Physics of Interacting Electrons in Disordered Systems* (Oxford University Press, Oxford, England, 1989), p. 2.
[32] N. F. Mott and E. A. Davis, *Electronic Processes in Non-Crystalline Materials* (Clarendon, Oxford, England, 1979), p. 105.
[33] P. W. Anderson, Phys. Rev. **124**, 41 (1961).
[34] J. Hubbard, Proc. R. Soc. A **276**, 238 (1963).
[35] P. I. Arseev, N. S. Maslova, V. I. Panov, and S. V. Savinov, J. Exp. Theor. Phys. **94**, 191 (2002).
[36] M. Berthe *et al.*, Phys. Rev. Lett. **97**, 206801 (2006).
[37] We note that a nonconstant tip density of states may influence experimental $I(V)$ spectra. To avoid such influence, we prepared metal-terminated apices on Cu(111) before taking spectra on GaAs.